

Study of the baryonic B decay $B^- \rightarrow \Sigma_c^{++} \bar{p} \pi^- \pi^-$

J. P. Lees,¹ V. Poireau,¹ V. Tisserand,¹ J. Garra Tico,² E. Grauges,² A. Palano^{ab,3} G. Eigen,⁴ B. Stugu,⁴
D. N. Brown,⁵ L. T. Kerth,⁵ Yu. G. Kolomensky,⁵ G. Lynch,⁵ H. Koch,⁶ T. Schroeder,⁶ D. J. Asgeirsson,⁷
C. Hearty,⁷ T. S. Mattison,⁷ J. A. McKenna,⁷ R. Y. So,⁷ A. Khan,⁸ V. E. Blinov,⁹ A. R. Buzykaev,⁹
V. P. Druzhinin,⁹ V. B. Golubev,⁹ E. A. Kravchenko,⁹ A. P. Onuchin,⁹ S. I. Serednyakov,⁹ Yu. I. Skovpen,⁹
E. P. Solodov,⁹ K. Yu. Todyshev,⁹ A. N. Yushkov,⁹ M. Bondioli,¹⁰ D. Kirkby,¹⁰ A. J. Lankford,¹⁰ M. Mandelkern,¹⁰
H. Atmacan,¹¹ J. W. Gary,¹¹ F. Liu,¹¹ O. Long,¹¹ G. M. Vitug,¹¹ C. Campagnari,¹² T. M. Hong,¹² D. Kovalskiy,¹²
J. D. Richman,¹² C. A. West,¹² A. M. Eisner,¹³ J. Kroseberg,¹³ W. S. Lockman,¹³ A. J. Martinez,¹³
B. A. Schumm,¹³ A. Seiden,¹³ D. S. Chao,¹⁴ C. H. Cheng,¹⁴ B. Echenard,¹⁴ K. T. Flood,¹⁴ D. G. Hitlin,¹⁴
P. Ongmongkolkul,¹⁴ F. C. Porter,¹⁴ A. Y. Rakitin,¹⁴ R. Andreassen,¹⁵ Z. Huard,¹⁵ B. T. Meadows,¹⁵
M. D. Sokoloff,¹⁵ L. Sun,¹⁵ P. C. Bloom,¹⁶ W. T. Ford,¹⁶ A. Gaz,¹⁶ U. Nauenberg,¹⁶ J. G. Smith,¹⁶ S. R. Wagner,¹⁶
R. Ayad,^{17,*} W. H. Toki,¹⁷ B. Spaan,¹⁸ K. R. Schubert,¹⁹ R. Schwierz,¹⁹ D. Bernard,²⁰ M. Verderi,²⁰ P. J. Clark,²¹
S. Playfer,²¹ D. Bettoni^{a,22} C. Bozzi^{a,22} R. Calabrese^{ab,22} G. Cibinetto^{ab,22} E. Fioravanti^{ab,22} I. Garzia^{ab,22}
E. Luppi^{ab,22} M. Munerato^{ab,22} M. Negrini^{ab,22} L. Piemontese^{a,22} V. Santoro^{a,22} R. Baldini-Ferrolì,²³
A. Calcaterra,²³ R. de Sangro,²³ G. Finocchiaro,²³ P. Patteri,²³ I. M. Peruzzi,^{23,†} M. Piccolo,²³ M. Rama,²³
A. Zallo,²³ R. Contri^{ab,24} E. Guido^{ab,24} M. Lo Vetere^{ab,24} M. R. Monge^{ab,24} S. Passaggio^{a,24} C. Patrignani^{ab,24}
E. Robutti^{a,24} B. Bhuyan,²⁵ V. Prasad,²⁵ C. L. Lee,²⁶ M. Morii,²⁶ A. J. Edwards,²⁷ A. Adametz,²⁸ U. Uwer,²⁸
H. M. Lacker,²⁹ T. Lueck,²⁹ P. D. Dauncey,³⁰ P. K. Behera,³¹ U. Mallik,³¹ C. Chen,³² J. Cochran,³² W. T. Meyer,³²
S. Prell,³² A. E. Rubin,³² A. V. Gritsan,³³ Z. J. Guo,³³ N. Arnaud,³⁴ M. Davier,³⁴ D. Derkach,³⁴ G. Grosdidier,³⁴
F. Le Diberder,³⁴ A. M. Lutz,³⁴ B. Malaescu,³⁴ P. Roudeau,³⁴ M. H. Schune,³⁴ A. Stocchi,³⁴ G. Wormser,³⁴
D. J. Lange,³⁵ D. M. Wright,³⁵ C. A. Chavez,³⁶ J. P. Coleman,³⁶ J. R. Fry,³⁶ E. Gabathuler,³⁶ D. E. Hutchcroft,³⁶
D. J. Payne,³⁶ C. Touramanis,³⁶ A. J. Bevan,³⁷ F. Di Lodovico,³⁷ R. Sacco,³⁷ M. Sigamani,³⁷ G. Cowan,³⁸
D. N. Brown,³⁹ C. L. Davis,³⁹ A. G. Denig,⁴⁰ M. Fritsch,⁴⁰ W. Gradl,⁴⁰ K. Griessinger,⁴⁰ A. Hafner,⁴⁰
E. Prencipe,⁴⁰ R. J. Barlow,^{41,‡} G. Jackson,⁴¹ G. D. Lafferty,⁴¹ E. Behn,⁴² R. Cenci,⁴² B. Hamilton,⁴²
A. Jawahery,⁴² D. A. Roberts,⁴² C. Dallapiccola,⁴³ R. Cowan,⁴⁴ D. Dujmic,⁴⁴ G. Sciolla,⁴⁴ R. Cheaib,⁴⁵
D. Lindemann,⁴⁵ P. M. Patel,^{45,§} S. H. Robertson,⁴⁵ P. Biassoni^{ab,46} N. Neri^{a,46} F. Palombo^{ab,46} S. Stracka^{ab,46}
L. Cremaldi,⁴⁷ R. Godang,^{47,¶} R. Kroeger,⁴⁷ P. Sonnek,⁴⁷ D. J. Summers,⁴⁷ X. Nguyen,⁴⁸ M. Simard,⁴⁸ P. Taras,⁴⁸
G. De Nardo^{ab,49} D. Monorchio^{ab,49} G. Onorato^{ab,49} C. Sciacca^{ab,49} M. Martinelli,⁵⁰ G. Raven,⁵⁰ C. P. Jessop,⁵¹
J. M. LoSecco,⁵¹ W. F. Wang,⁵¹ K. Honscheid,⁵² R. Kass,⁵² J. Brau,⁵³ R. Frey,⁵³ N. B. Sinev,⁵³ D. Strom,⁵³
E. Torrence,⁵³ E. Feltresi^{ab,54} N. Gagliardi^{ab,54} M. Margoni^{ab,54} M. Morandin^{a,54} M. Posocco^{a,54} M. Rotondo^{a,54}
G. Simi^{a,54} F. Simonetto^{ab,54} R. Stroili^{ab,54} S. Akar,⁵⁵ E. Ben-Haim,⁵⁵ M. Bomben,⁵⁵ G. R. Bonneaud,⁵⁵
H. Briand,⁵⁵ G. Calderini,⁵⁵ J. Chauveau,⁵⁵ O. Hamon,⁵⁵ Ph. Leruste,⁵⁵ G. Marchiori,⁵⁵ J. Ocariz,⁵⁵ S. Sitt,⁵⁵
M. Biasini^{ab,56} E. Manoni^{ab,56} S. Pacetti^{ab,56} A. Rossi^{ab,56} C. Angelini^{ab,57} G. Batignani^{ab,57} S. Bettarini^{ab,57}
M. Carpinelli^{ab,57,**} G. Casarosa^{ab,57} A. Cervelli^{ab,57} F. Forti^{ab,57} M. A. Giorgi^{ab,57} A. Lusiani^{ac,57} B. Oberhof^{ab,57}
E. Paoloni^{ab,57} A. Perez^{a,57} G. Rizzo^{ab,57} J. J. Walsh^{a,57} D. Lopes Pegna,⁵⁸ J. Olsen,⁵⁸ A. J. S. Smith,⁵⁸
A. V. Telnov,⁵⁸ F. Anulli^{a,59} R. Faccini^{ab,59} F. Ferrarotto^{a,59} F. Ferroni^{ab,59} M. Gaspero^{ab,59} L. Li Gioi^{a,59}
M. A. Mazzoni^{a,59} G. Piredda^{a,59} C. Büniger,⁶⁰ O. Grünberg,⁶⁰ T. Hartmann,⁶⁰ T. Leddig,⁶⁰ H. Schröder,^{60,§}
C. Voss,⁶⁰ R. Waldi,⁶⁰ T. Adye,⁶¹ E. O. Olaiya,⁶¹ F. F. Wilson,⁶¹ S. Emery,⁶² G. Hamel de Monchenault,⁶²
G. Vasseur,⁶² Ch. Yèche,⁶² D. Aston,⁶³ D. J. Bard,⁶³ R. Bartoldus,⁶³ J. F. Benitez,⁶³ C. Cartaro,⁶³ M. R. Convery,⁶³
J. Dorfan,⁶³ G. P. Dubois-Felsmann,⁶³ W. Dunwoodie,⁶³ M. Ebert,⁶³ R. C. Field,⁶³ M. Franco Sevilla,⁶³
B. G. Fulsom,⁶³ A. M. Gabareen,⁶³ M. T. Graham,⁶³ P. Grenier,⁶³ C. Hast,⁶³ W. R. Innes,⁶³ M. H. Kelsey,⁶³
P. Kim,⁶³ M. L. Kocian,⁶³ D. W. G. S. Leith,⁶³ P. Lewis,⁶³ B. Lindquist,⁶³ S. Luitz,⁶³ V. Luth,⁶³ H. L. Lynch,⁶³
D. B. MacFarlane,⁶³ D. R. Muller,⁶³ H. Neal,⁶³ S. Nelson,⁶³ M. Perl,⁶³ T. Pulliam,⁶³ B. N. Ratcliff,⁶³ A. Roodman,⁶³
A. A. Salnikov,⁶³ R. H. Schindler,⁶³ A. Snyder,⁶³ D. Su,⁶³ M. K. Sullivan,⁶³ J. Va'vra,⁶³ A. P. Wagner,⁶³
W. J. Wisniewski,⁶³ M. Wittgen,⁶³ D. H. Wright,⁶³ H. W. Wulsin,⁶³ C. C. Young,⁶³ V. Ziegler,⁶³ W. Park,⁶⁴

M. V. Purohit,⁶⁴ R. M. White,⁶⁴ J. R. Wilson,⁶⁴ A. Randle-Conde,⁶⁵ S. J. Sekula,⁶⁵ M. Bellis,⁶⁶ P. R. Burchat,⁶⁶ T. S. Miyashita,⁶⁶ M. S. Alam,⁶⁷ J. A. Ernst,⁶⁷ R. Gorodeisky,⁶⁸ N. Guttman,⁶⁸ D. R. Peimer,⁶⁸ A. Soffer,⁶⁸ P. Lund,⁶⁹ S. M. Spanier,⁶⁹ J. L. Ritchie,⁷⁰ A. M. Ruland,⁷⁰ R. F. Schwitters,⁷⁰ B. C. Wray,⁷⁰ J. M. Izen,⁷¹ X. C. Lou,⁷¹ F. Bianchi^{ab},⁷² D. Gamba^{ab},⁷² L. Lancieri^{ab},⁷³ L. Vitale^{ab},⁷³ F. Martinez-Vidal,⁷⁴ A. Oyanguren,⁷⁴ H. Ahmed,⁷⁵ J. Albert,⁷⁵ Sw. Banerjee,⁷⁵ F. U. Bernlochner,⁷⁵ H. H. F. Choi,⁷⁵ G. J. King,⁷⁵ R. Kowalewski,⁷⁵ M. J. Lewczuk,⁷⁵ I. M. Nugent,⁷⁵ J. M. Roney,⁷⁵ R. J. Sobie,⁷⁵ N. Tasneem,⁷⁵ T. J. Gershon,⁷⁶ P. F. Harrison,⁷⁶ T. E. Latham,⁷⁶ E. M. T. Puccio,⁷⁶ H. R. Band,⁷⁷ S. Dasu,⁷⁷ Y. Pan,⁷⁷ R. Prepost,⁷⁷ and S. L. Wu⁷⁷

(The BABAR Collaboration)

¹Laboratoire d'Annecy-le-Vieux de Physique des Particules (LAPP),
Université de Savoie, CNRS/IN2P3, F-74941 Annecy-Le-Vieux, France

²Universitat de Barcelona, Facultat de Física, Departament ECM, E-08028 Barcelona, Spain

³INFN Sezione di Bari^a; Dipartimento di Fisica, Università di Bari^b, I-70126 Bari, Italy

⁴University of Bergen, Institute of Physics, N-5007 Bergen, Norway

⁵Lawrence Berkeley National Laboratory and University of California, Berkeley, California 94720, USA

⁶Ruhr Universität Bochum, Institut für Experimentalphysik 1, D-44780 Bochum, Germany

⁷University of British Columbia, Vancouver, British Columbia, Canada V6T 1Z1

⁸Brunel University, Uxbridge, Middlesex UB8 3PH, United Kingdom

⁹Budker Institute of Nuclear Physics, Novosibirsk 630090, Russia

¹⁰University of California at Irvine, Irvine, California 92697, USA

¹¹University of California at Riverside, Riverside, California 92521, USA

¹²University of California at Santa Barbara, Santa Barbara, California 93106, USA

¹³University of California at Santa Cruz, Institute for Particle Physics, Santa Cruz, California 95064, USA

¹⁴California Institute of Technology, Pasadena, California 91125, USA

¹⁵University of Cincinnati, Cincinnati, Ohio 45221, USA

¹⁶University of Colorado, Boulder, Colorado 80309, USA

¹⁷Colorado State University, Fort Collins, Colorado 80523, USA

¹⁸Technische Universität Dortmund, Fakultät Physik, D-44221 Dortmund, Germany

¹⁹Technische Universität Dresden, Institut für Kern- und Teilchenphysik, D-01062 Dresden, Germany

²⁰Laboratoire Leprince-Ringuet, Ecole Polytechnique, CNRS/IN2P3, F-91128 Palaiseau, France

²¹University of Edinburgh, Edinburgh EH9 3JZ, United Kingdom

²²INFN Sezione di Ferrara^a; Dipartimento di Fisica, Università di Ferrara^b, I-44100 Ferrara, Italy

²³INFN Laboratori Nazionali di Frascati, I-00044 Frascati, Italy

²⁴INFN Sezione di Genova^a; Dipartimento di Fisica, Università di Genova^b, I-16146 Genova, Italy

²⁵Indian Institute of Technology Guwahati, Guwahati, Assam, 781 039, India

²⁶Harvard University, Cambridge, Massachusetts 02138, USA

²⁷Harvey Mudd College, Claremont, California 91711, USA

²⁸Universität Heidelberg, Physikalisches Institut, Philosophenweg 12, D-69120 Heidelberg, Germany

²⁹Humboldt-Universität zu Berlin, Institut für Physik, Newtonstr. 15, D-12489 Berlin, Germany

³⁰Imperial College London, London, SW7 2AZ, United Kingdom

³¹University of Iowa, Iowa City, Iowa 52242, USA

³²Iowa State University, Ames, Iowa 50011-3160, USA

³³Johns Hopkins University, Baltimore, Maryland 21218, USA

³⁴Laboratoire de l'Accélérateur Linéaire, IN2P3/CNRS et Université Paris-Sud 11,
Centre Scientifique d'Orsay, B. P. 34, F-91898 Orsay Cedex, France

³⁵Lawrence Livermore National Laboratory, Livermore, California 94550, USA

³⁶University of Liverpool, Liverpool L69 7ZE, United Kingdom

³⁷Queen Mary, University of London, London, E1 4NS, United Kingdom

³⁸University of London, Royal Holloway and Bedford New College, Egham, Surrey TW20 0EX, United Kingdom

³⁹University of Louisville, Louisville, Kentucky 40292, USA

⁴⁰Johannes Gutenberg-Universität Mainz, Institut für Kernphysik, D-55099 Mainz, Germany

⁴¹University of Manchester, Manchester M13 9PL, United Kingdom

⁴²University of Maryland, College Park, Maryland 20742, USA

⁴³University of Massachusetts, Amherst, Massachusetts 01003, USA

⁴⁴Massachusetts Institute of Technology, Laboratory for Nuclear Science, Cambridge, Massachusetts 02139, USA

⁴⁵McGill University, Montréal, Québec, Canada H3A 2T8

⁴⁶INFN Sezione di Milano^a; Dipartimento di Fisica, Università di Milano^b, I-20133 Milano, Italy

⁴⁷University of Mississippi, University, Mississippi 38677, USA

⁴⁸Université de Montréal, Physique des Particules, Montréal, Québec, Canada H3C 3J7

⁴⁹INFN Sezione di Napoli^a; Dipartimento di Scienze Fisiche,
Università di Napoli Federico II^b, I-80126 Napoli, Italy

⁵⁰NIKHEF, National Institute for Nuclear Physics and High Energy Physics, NL-1009 DB Amsterdam, The Netherlands

- ⁵¹University of Notre Dame, Notre Dame, Indiana 46556, USA
⁵²Ohio State University, Columbus, Ohio 43210, USA
⁵³University of Oregon, Eugene, Oregon 97403, USA
⁵⁴INFN Sezione di Padova^a; Dipartimento di Fisica, Università di Padova^b, I-35131 Padova, Italy
⁵⁵Laboratoire de Physique Nucléaire et de Hautes Energies, IN2P3/CNRS, Université Pierre et Marie Curie-Paris6, Université Denis Diderot-Paris7, F-75252 Paris, France
⁵⁶INFN Sezione di Perugia^a; Dipartimento di Fisica, Università di Perugia^b, I-06100 Perugia, Italy
⁵⁷INFN Sezione di Pisa^a; Dipartimento di Fisica, Università di Pisa^b; Scuola Normale Superiore di Pisa^c, I-56127 Pisa, Italy
⁵⁸Princeton University, Princeton, New Jersey 08544, USA
⁵⁹INFN Sezione di Roma^a; Dipartimento di Fisica, Università di Roma La Sapienza^b, I-00185 Roma, Italy
⁶⁰Universität Rostock, D-18051 Rostock, Germany
⁶¹Rutherford Appleton Laboratory, Chilton, Didcot, Oxon, OX11 0QX, United Kingdom
⁶²CEA, Irfu, SPP, Centre de Saclay, F-91191 Gif-sur-Yvette, France
⁶³SLAC National Accelerator Laboratory, Stanford, California 94309 USA
⁶⁴University of South Carolina, Columbia, South Carolina 29208, USA
⁶⁵Southern Methodist University, Dallas, Texas 75275, USA
⁶⁶Stanford University, Stanford, California 94305-4060, USA
⁶⁷State University of New York, Albany, New York 12222, USA
⁶⁸Tel Aviv University, School of Physics and Astronomy, Tel Aviv, 69978, Israel
⁶⁹University of Tennessee, Knoxville, Tennessee 37996, USA
⁷⁰University of Texas at Austin, Austin, Texas 78712, USA
⁷¹University of Texas at Dallas, Richardson, Texas 75083, USA
⁷²INFN Sezione di Torino^a; Dipartimento di Fisica Sperimentale, Università di Torino^b, I-10125 Torino, Italy
⁷³INFN Sezione di Trieste^a; Dipartimento di Fisica, Università di Trieste^b, I-34127 Trieste, Italy
⁷⁴IFIC, Universitat de Valencia-CSIC, E-46071 Valencia, Spain
⁷⁵University of Victoria, Victoria, British Columbia, Canada V8W 3P6
⁷⁶Department of Physics, University of Warwick, Coventry CV4 7AL, United Kingdom
⁷⁷University of Wisconsin, Madison, Wisconsin 53706, USA

We report the measurement of the baryonic B decay $B^- \rightarrow \Sigma_c^{++} \bar{p} \pi^- \pi^-$. Using a data sample of $467 \times 10^6 B\bar{B}$ pairs collected with the BABAR detector at the PEP-II storage ring at SLAC, the measured branching fraction is $(2.98 \pm 0.16_{(\text{stat})} \pm 0.15_{(\text{syst})} \pm 0.77_{(\Lambda_c)}) \times 10^{-4}$, where the last error is due to the uncertainty in $\mathcal{B}(\Lambda_c^+ \rightarrow pK^- \pi^+)$. The data suggest the existence of resonant subchannels $B^- \rightarrow \Lambda_c(2595)^+ \bar{p} \pi^-$ and, possibly, $B^- \rightarrow \Sigma_c^{++} \bar{\Delta}^- \pi^-$. We see unexplained structures in $m(\Sigma_c^{++} \pi^- \pi^-)$ at $3.25 \text{ GeV}/c^2$, $3.8 \text{ GeV}/c^2$, and $4.2 \text{ GeV}/c^2$.

PACS numbers: 13.25.Hw, 13.60.Rj, 14.20.Lq

I. Introduction

The large mass of the B meson allows a wide spectrum of baryonic decays, which have, in total, a branching fraction of $(6.8 \pm 0.6)\%$ [1]. This makes B decays a good place to study the mechanisms of baryon production. One approach to investigate the baryonization process in B decays is to measure and compare their exclusive branching fractions and study the dynamic structure of the decay, i.e., the influence of resonant subchannels.

In this paper, we present a study of the decay $B^- \rightarrow \Sigma_c^{++} \bar{p} \pi^- \pi^-$ [2]. This decay is a resonant subchannel of the five body final state $B^- \rightarrow \Lambda_c^+ \bar{p} \pi^+ \pi^- \pi^-$, which has the largest hitherto known branching fraction among all baryonic B decays and hence is a good starting point for further investigations. The analyzed decay can be compared with $B^- \rightarrow \Sigma_c^0 \bar{p} \pi^+ \pi^-$ and $\bar{B}^0 \rightarrow \Sigma_c^{++} \bar{p} \pi^-$, which have similar quark content and phase space.

Large differences between the branching fractions of $B^- \rightarrow \Sigma_c^{++} \bar{p} \pi^- \pi^-$, $B^- \rightarrow \Sigma_c^0 \bar{p} \pi^+ \pi^-$, and

$\bar{B}^0 \rightarrow \Sigma_c^{++} \bar{p} \pi^-$ could indicate a considerable impact of intermediate states on baryonic B decays. For example the decay $B^- \rightarrow \Sigma_c^0 \bar{p} \pi^+ \pi^-$ allows a number of resonant three-body decays (including \bar{N} , $\bar{\Delta}^0$, and ρ^0 resonances) that cannot occur in $B^- \rightarrow \Sigma_c^{++} \bar{p} \pi^- \pi^-$. The importance of resonant subchannels can be quantified, e.g., by the ratio of $[\mathcal{B}(B^- \rightarrow \Sigma_c^{++} \bar{p} \pi^- \pi^-) + \mathcal{B}(B^- \rightarrow \Sigma_c^0 \bar{p} \pi^+ \pi^-)] / \mathcal{B}(B^- \rightarrow \Lambda_c^+ \bar{p} \pi^+ \pi^- \pi^-)$.

The CLEO Collaboration measured $\mathcal{B}(B^- \rightarrow \Lambda_c^+ \bar{p} \pi^+ \pi^- \pi^-) = (22.5 \pm 3.5 \pm 5.8) \times 10^{-4}$ and $\mathcal{B}(B^- \rightarrow \Sigma_c^0 \bar{p} \pi^+ \pi^-) = (4.4 \pm 1.7 \pm 1.1) \times 10^{-4}$ [3]. The decay $\bar{B}^0 \rightarrow \Sigma_c^{++} \bar{p} \pi^-$ was measured by the CLEO [3] and the Belle [4] Collaborations. The Particle Data Group has calculated an average of $\mathcal{B}(\bar{B}^0 \rightarrow \Sigma_c^{++} \bar{p} \pi^-) = (2.2 \pm 0.7 \pm 0.6) \times 10^{-4}$ [1]. For all these branching fractions the first uncertainty is the combined statistical and systematic error and the second one is due to the uncertainty in $\mathcal{B}(\Lambda_c^+ \rightarrow pK^- \pi^+) = (5.0 \pm 1.3)\%$ [1].

II. The *BABAR* experiment

This analysis is based on a dataset of about 426 fb^{-1} , corresponding to $467 \times 10^6 B\bar{B}$ pairs. The sample was collected with the *BABAR* detector at the PEP-II asymmetric-energy e^+e^- storage ring, which was operated at a center-of-mass energy equal to the $\Upsilon(4S)$ mass. For generation of Monte Carlo (MC) simulated data we use *EvtGen* [5] for event generation and *GEANT4* [6] for detector simulation.

The *BABAR* detector is described in detail elsewhere [7]. The selection of proton, kaon, and pion candidates is based on measurements of the energy loss in the silicon vertex tracker and the drift chamber, and of the Cherenkov radiation in the detector of internally reflected Cherenkov light [8]. The average efficiency for pion identification is approximately 95%, with a typical misidentification rate of 10% due to other charged particles such as muons and kaons, depending on the momentum and the polar angle of the particle. The efficiency for kaon identification is about 95% with a misidentification rate less than 5% due to protons and pions. The efficiency for proton and antiproton identification is about 90% with a misidentification rate about 2% due to kaons.

III. Decay reconstruction

The decay $B^- \rightarrow \Sigma_c^{++} \bar{p} \pi^- \pi^-$ is reconstructed in the subchannel $\Sigma_c^{++} \rightarrow \Lambda_c^+ \pi^+$, $\Lambda_c^+ \rightarrow p K^- \pi^+$. For the reconstruction of the B candidate the entire decay tree is fitted simultaneously. A vertex fit is performed for B^- , Σ_c^{++} , and Λ_c^+ , and the χ^2 fit probability is required to exceed 0.1%.

To suppress background, the invariant mass of the $pK^-\pi^+$ combination is required to satisfy $2275 \text{ MeV}/c^2 < m_{pK^-\pi^+} < 2296 \text{ MeV}/c^2$, i.e., compatible with coming from the decay $\Lambda_c^+ \rightarrow p K^- \pi^+$. This selection corresponds to 2.8 times the observed width of reconstructed Λ_c^+ candidates which are centered at $m_{pK^-\pi^+} = 2285.4 \text{ MeV}/c^2$. The separation of signal from background in the B -candidate sample is obtained using two kinematic variables, $\Delta E = E_B^* - \sqrt{s}/2$ and $m_{\text{ES}} = \sqrt{(s/2 + \mathbf{p}_i \cdot \mathbf{p}_B)^2/E_i^2 - |\mathbf{p}_B|^2}$, where \sqrt{s} is the center-of-mass (CM) energy of the e^+e^- pair and E_B^* the energy of the B candidate in the CM system. (E_i, \mathbf{p}_i) is the four-momentum vector of the e^+e^- CM system and \mathbf{p}_B the B -candidate momentum vector, both measured in the laboratory frame. For correctly reconstructed B decays, m_{ES} is centered at the B meson mass and ΔE is centered at zero. Throughout this analysis, B candidates are required to have m_{ES} within 8 MeV (3.4σ) of the measured B mass of $m_{\text{ES}} = 5279.1 \text{ MeV}$.

Figure 1 shows the distribution of $\Delta M \equiv m(\Lambda_c^+ \pi^+) - m(\Lambda_c^+)$ in data for candidates that satisfy the criteria described above for m_{ES} and $m_{pK^-\pi^+}$ and for which ΔE is between -60 MeV and $+40 \text{ MeV}$. We perform a binned

minimum χ^2 fit using a second-order polynomial for the description of the background and the sum of a Voigt distribution (the convolution of a Breit-Wigner function with a Gaussian function) and a Gaussian to parametrize the Σ_c^{++} signal. A detailed explanation of the fit function is given in Sec. IV. The fitted Σ_c^{++} signal yield is $N = 1020 \pm 95$.

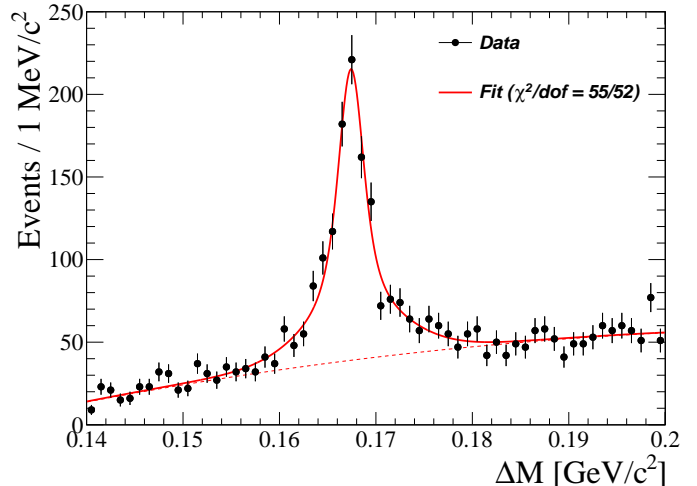


FIG. 1: Fitted ΔM distribution for B candidates in data. All candidates are required to satisfy the selection criteria on m_{ES} , $m_{pK^-\pi^+}$, and ΔE .

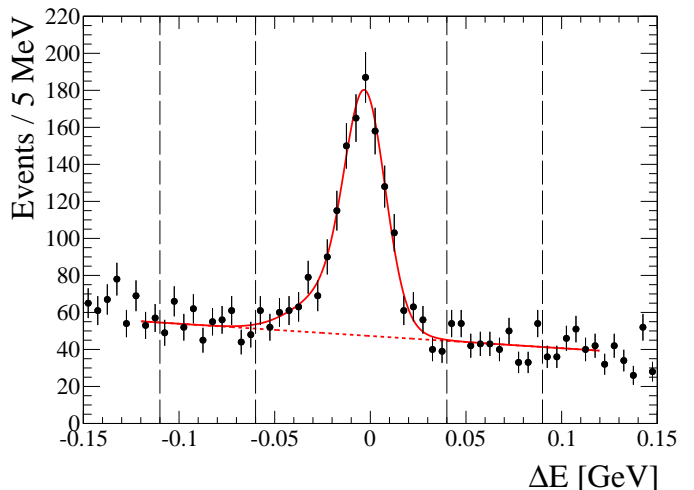


FIG. 2: Fitted ΔE distribution in data with selection criteria applied to $m_{pK^-\pi^+}$, m_{ES} , and ΔM . The goodness of the fit is $\chi^2/\text{dof} = 36/40$. The ΔE signal region is between -60 MeV and 40 MeV , and enclosed by the two sideband regions that each have a width of 50 MeV .

Figure 2 shows the ΔE distribution in data for candidates that satisfy the criteria described above for m_{ES} and $m_{pK^-\pi^+}$ and for which ΔM is between $0.157 \text{ GeV}/c^2$ and $0.178 \text{ GeV}/c^2$. The latter is a selection of Σ_c^{++} candidates with an efficiency of 92% in signal MC.

In the binned minimum χ^2 fit we use the sum of two Gaussian functions for the signal and a linear function for the background. The second Gaussian accommodates B decays with missing energy due to final state radiation. Each Gaussian has a mean parameter (μ) and a standard deviation (σ). The joint normalization is described by N_{sig} and the fraction of the first Gaussian is f_1 . We parametrize the background shape of the ΔE distribution as a first-order polynomial which provides a good description of the ΔE distribution for candidates in the m_{ES} sideband in the range $5.20 \text{ GeV}/c^2 < m_{\text{ES}} < 5.26 \text{ GeV}/c^2$. All parameters are permitted to vary during fitting. Table I presents the resulting signal parameters. The signal yield is 840 ± 55 events.

TABLE I: The parameters for the double-Gaussian function describing the signal contribution in the fit to the ΔE distribution shown in Fig. 2. f_1 is the fraction of the signal in the narrower Gaussian.

Parameter	Fit result
N_{sig}	840 ± 55
f_1	$(70 \pm 23)\%$
μ_1	$(-2.7 \pm 1.2) \text{ MeV}$
σ_1	$(10 \pm 1.6) \text{ MeV}$
μ_2	$(-16 \pm 14) \text{ MeV}$
σ_2	$(20 \pm 5.6) \text{ MeV}$

IV. Signal extraction

There are two sources of background that contribute to the signal in ΔE and ΔM . The first one is B decays that have the same final state, in particular $B^- \rightarrow \Lambda_c^+ \bar{p} \pi^+ \pi^- \pi^-$, and the other one is B decays that have a Σ_c^{++} among its decay products, e.g., $\bar{B}^0 \rightarrow \Sigma_c^{++} \bar{p} \pi^- \pi^0$. To reject this background we make a binwise fit using ΔM as a discriminating variable to create a background-subtracted ΔE distribution from which we extract the true signal yield in order to determine $\mathcal{B}(B^- \rightarrow \Sigma_c^{++} \bar{p} \pi^- \pi^-)$. The binwise fitting procedure is described in the following paragraph.

After applying the selection in $m_{pK^- \pi^+}$ and m_{ES} (no selection in ΔM), we divide the ΔE range $(-105, 105) \text{ MeV}$ into 14 equal slices and fit the ΔM distribution in each slice separately in the range $0.14 \text{ GeV}/c^2 < \Delta M < 0.2 \text{ GeV}/c^2$. In the fits the Σ_c^{++} signal is represented by the sum of a Voigt function and a Gaussian function. The Voigt distribution has four parameters ($N_{\text{sig}}, \mu, \Gamma, \sigma$) and models the signal peak region, where μ is the mean of the Voigt and represents the Σ_c^{++} mass, which is fixed to the value obtained from an inclusive analysis of $\Sigma_c^{++} \rightarrow \Lambda_c^+ \pi^+$ candidates in the data. The parameter Γ is the intrinsic width of the Σ_c^{++} and is fixed to the 2010 Review of Particle Properties

(RPP) value [1], and σ describes the detector resolution in ΔM for the Σ_c^{++} determined, independently for each ΔE slice, from the signal MC. The remaining parameter N_{sig}^i is the fitted Σ_c^{++} signal yield in each of the ΔE bins.

There is a correlation between ΔM and ΔE that is very prominent due to the inaccurate momentum measurement of the slow π^+ from the Σ_c^{++} decay. As a result the Σ_c^{++} signal has tails in the ΔM distribution that are modeled by the Gaussian function whose parameters are determined, independently for each ΔE slice, from the signal MC. The background is represented by a second-order polynomial. This shape was determined from the sidebands $|\Delta E| \in (50, 300) \text{ MeV}$ and, compared to the other polynomials, gives the best χ^2 fit probability. The fits in ΔM determine the background level and the number of Σ_c^{++} baryons.

Figure 3 shows the Σ_c^{++} signal yield as a function of ΔE . We fit this distribution with the same functions described in Sec. III and fix the signal parameters, except for N_{sig} , to those determined there. The true signal yield is $N_{\text{sig}} = 787 \pm 43$ events.

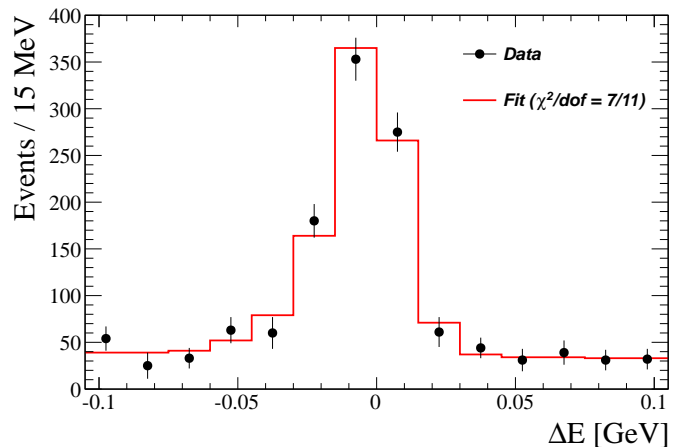


FIG. 3: ΔE distribution for $B^- \rightarrow \Sigma_c^{++} \bar{p} \pi^- \pi^-$ candidates in data. The points with error bars represent the number of Σ_c^{++} candidates N_{sig}^i from a fit to $\Delta M \equiv m(\Lambda_c^+ \pi^+) - m(\Lambda_c^+)$. All signal parameters for the ΔE distribution, except N_{sig} , are fixed to those shown in Table I.

V. Efficiency

The efficiency is calculated from the simulated events. These events were generated uniformly in four-body phase space (PS), but the actual decay distribution is, a priori, unknown. Therefore, when calculating the efficiency, we weight the MC events so that we reproduce the distributions of the two-body invariant mass distributions for the decay products of the B candidates in data. The resulting efficiency is checked by repeating the procedure using the three-body masses and then again using the angles between the B daughters in the B rest

frame. The different procedures give an average efficiency of $(11.3 \pm 0.2_{(\text{syst})})\%$, which is used to determine the branching fraction. Out of the efficiencies from the different procedures, we use the maximum deviation from the average efficiency as systematic uncertainty. The statistical uncertainty, due to the use of the data, is negligible compared to the statistical uncertainty in the event yield. The efficiency calculated using unweighted events is 11.0%.

VI. Systematic uncertainties

We estimate the uncertainty on the signal extraction in three different ways: (1) the fit to ΔE in Fig. 3 is repeated separately for each shape parameter in Table I, while permitting this parameter to float. The absolute deviations (δN) in the event yield to our true signal yield $N_{\text{sig}} = 787$ add up to 23 (see Table II). (2) We use a second-order polynomial for the background while letting all other parameters fixed ($\delta N = 5$), and (3) we fit only the background with a first-order polynomial and subtract its integral from the histogram content in the range $-60 \text{ MeV} < \Delta E < 45 \text{ MeV}$ in order to obtain an alternative signal yield ($\delta N = 3$). The absolute values of the deviations in the event yields from all of these variations add up to 31. The resulting relative uncertainty on the signal yield is 4.0%. Other systematic errors come from track reconstruction efficiency (2.4%) [9], efficiency (1.8%), and the number of produced $B\bar{B}$ pairs in the data sample (1.1%). The total relative uncertainty on the branching fraction is 5.1%.

TABLE II: The results of the fits to ΔE in Fig. 3 while the given parameter is allowed to float. δN is the absolute deviation to our true signal yield $N_{\text{sig}} = 787$.

Floating parameter	Fit result	δN
f_1	$(70 \pm 7.7)\%$	2
μ_1	$(-2.8 \pm 1.0) \text{ MeV}$	0
σ_1	$(11 \pm 0.9) \text{ MeV}$	8
μ_2	$(-15 \pm 5.2) \text{ MeV}$	2
σ_2	$(18 \pm 4.6) \text{ MeV}$	11

VII. Branching fraction results

Using the results from the signal extraction, efficiency determination, and estimation of systematic errors we find

$$\mathcal{B}(B^- \rightarrow \Sigma_c^{++} \bar{p} \pi^- \pi^-) \cdot \mathcal{B}(\Lambda_c^+ \rightarrow p K^- \pi^+) = \frac{N_{\text{sig}}}{\varepsilon \cdot N_{B\bar{B}}} \\ = (1.49 \pm 0.08_{(\text{stat})} \pm 0.08_{(\text{syst})}) \times 10^{-5}, \text{ and} \quad (1)$$

$$\mathcal{B}(B^- \rightarrow \Sigma_c^{++} \bar{p} \pi^- \pi^-) = \frac{N_{\text{sig}}}{\varepsilon \cdot N_{B\bar{B}} \cdot \mathcal{B}(\Lambda_c^+ \rightarrow p K^- \pi^+)} \\ = (2.98 \pm 0.16_{(\text{stat})} \pm 0.15_{(\text{syst})} \pm 0.77_{(\Lambda_c)}) \times 10^{-4}. \quad (2)$$

In Eq. 2 the last error is due to the uncertainty in $\mathcal{B}(\Lambda_c^+ \rightarrow p K^- \pi^+)$.

VIII. Fraction of PS distributed decays

To compare the two-body and three-body invariant masses of the B decay products in data with PS, we determine an effective PS fraction of the total branching ratio. To do this, we assume that the resonant substructures are due to the intermediate states $\Lambda_c^{*+} \rightarrow \Sigma_c^{++} \pi^-$ and $\bar{\Delta}^{--} \rightarrow \bar{p} \pi^-$, and the remainder is distributed according to four-body PS. We investigate all two-dimensional planes that are spanned by the two-body invariant masses of the B decay products, e.g. $m(\Sigma_c^{++} \pi_s^-)$ against $m(\bar{p} \pi_f^-)$, to look for a range that is free from Λ_c^{*+} and $\bar{\Delta}^{--}$ resonances and hence can be described by a four-body PS distribution. The symbol π_s^- refers to the π^- that has the lower momentum in the e^+e^- CM system. The other π^- is denoted as π_f^- . We see no indication of $\bar{\Delta}^{--}$ and Λ_c^{*+} resonances for B candidates in the range $3.050 \text{ GeV}/c^2 < m(\Sigma_c^{++} \pi_s^-) < 3.450 \text{ GeV}/c^2$, where the normalization of the PS distribution is determined by fitting the sideband-subtracted data (Fig. 4).

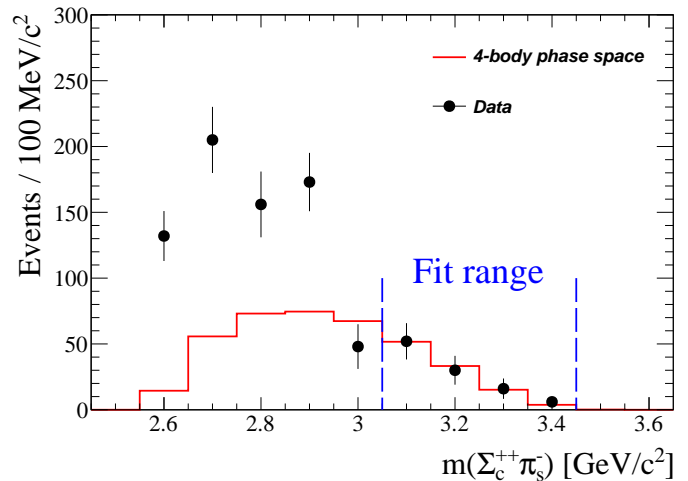


FIG. 4: The $m(\Sigma_c^{++} \pi_s^-)$ distribution in data (points with error bars) and for simulated four-body phase space decays (histogram). The distribution in data results from a sideband subtraction in ΔE according to the definition in Fig. 2.

From the ratio of the efficiency-corrected integrals of the distributions in Fig.4, we calculate an effective PS fraction:

$$\frac{\mathcal{B}(B^- \rightarrow \Sigma_c^{++} \bar{p} \pi^- \pi^-)_{\text{PS}}}{\mathcal{B}(B^- \rightarrow \Sigma_c^{++} \bar{p} \pi^- \pi^-)} = \frac{389}{11.0\%} \cdot \frac{11.3\%}{816} = 49\%. \quad (3)$$

This percentage will be used to normalize the PS projection in the two-body and three-body invariant mass distributions in Figs. 5–7.

IX. Resonant subchannels

Figure 5 shows the invariant mass distribution of $\bar{p}\pi^- = \{\bar{p}\pi_s^-, \bar{p}\pi_f^-\}$ [sum of the distributions of $m(\bar{p}\pi_s^-)$ and $m(\bar{p}\pi_f^-)$] after sideband subtraction in ΔE (see Fig. 2 for the definition of the sidebands) and efficiency correction. The efficiency correction here and in the other invariant masses of the B daughters is determined from PS MC for the particular mass that is considered. The differences between data and PS in the range $m(\bar{p}\pi^-) \in (1.2, 1.7) \text{ GeV}/c^2$ are compatible with the existence of the resonances $\bar{\Delta}^{--}$ (1232, 1600, 1620).

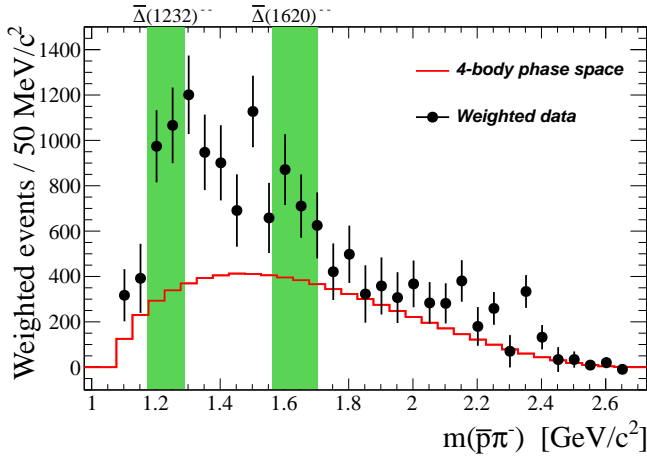


FIG. 5: The $m(\bar{p}\pi^-)$ distribution in data and simulated four-body phase space decays. The shaded vertical ranges represent a width of one Γ and are centered at the average mass of $\bar{\Delta}^{--}$ (1232) and $\bar{\Delta}^{--}$ (1620), respectively. The parameters are taken from the RPP [1]. The range of $\bar{\Delta}^{--}$ (1600) is not drawn since its parameters have large uncertainties.

Figure 6 shows the invariant mass of $\Sigma_c^{++}\pi^- = \{\Sigma_c^{++}\pi_s^-, \Sigma_c^{++}\pi_f^-\}$ after efficiency correction and sideband subtraction in ΔE . The large number of events at threshold are consistent with the decay $B^- \rightarrow \Lambda_c(2595)^+ \bar{p}\pi^-$. There are no significant signals for other Λ_c^{*+} resonances.

In the three-body invariant mass distribution $m(\Sigma_c^{++}\pi^-\pi^-)$ (Fig. 7) we see unexplained structures at $3.25 \text{ GeV}/c^2$, $3.8 \text{ GeV}/c^2$, and $4.2 \text{ GeV}/c^2$. However, because of the limited number of signal candidates, it is not possible to analyze these enhancements in more detail.

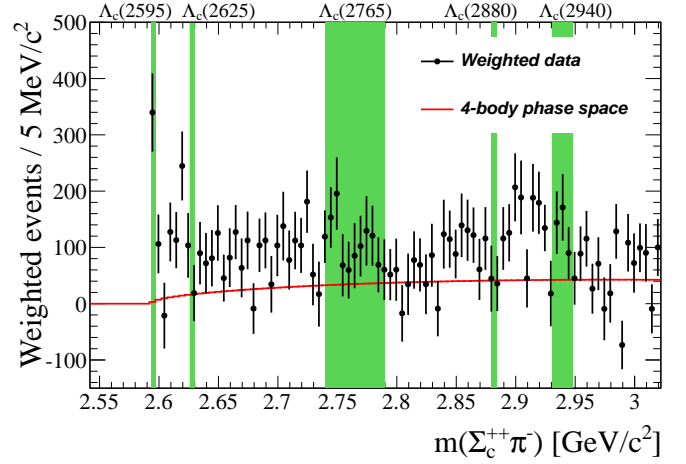


FIG. 6: The $m(\Sigma_c^{++}\pi^-)$ distribution in data after efficiency correction and ΔE -sideband subtraction. The solid line shows four-body phase space decays. The shaded vertical ranges represent a width of one Γ and are centered at the average mass of the respective Λ_c^{*+} resonance. The parameters are taken from the RPP [1].

We find no indication of a threshold enhancement in the baryon-antibaryon mass distribution.

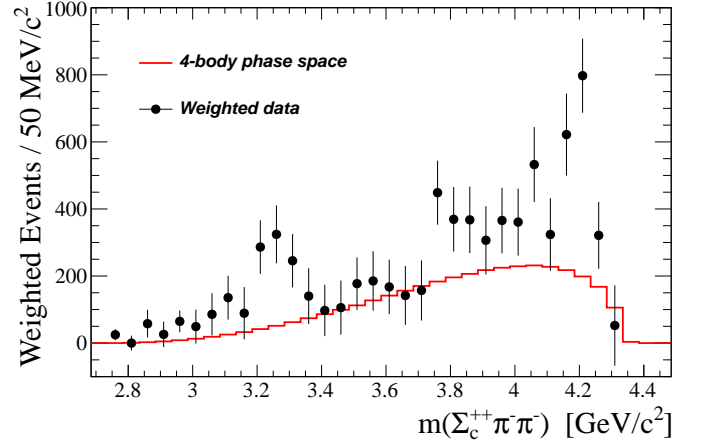


FIG. 7: The $m(\Sigma_c^{++}\pi^-\pi^-)$ distribution in data and simulated four-body phase space decays. The histogram in data includes efficiency correction and ΔE -sideband subtraction according to the definition in Fig. 2.

X. Summary and Conclusions

We have measured the branching fraction $\mathcal{B}(B^- \rightarrow \Sigma_c^{++} \bar{p} \pi^- \pi^-) = (2.98 \pm 0.22 \pm 0.77_{(\Lambda_c)}) \times 10^{-4}$. This improves on the previous measurement by CLEO [3].

We have calculated an effective PS fraction of 49% for the observed decay, which may indicate the importance of resonant substructures in baryonic B decays. By comparing the data and four-body PS in the distributions of

the invariant masses of the B daughters, we find suggestions for the resonant subchannels $B^- \rightarrow \Lambda_c(2595)^+ \bar{p}\pi^-$ and, possibly, $B^- \rightarrow \Sigma_c^{++} \bar{\Delta}^{--} \pi^-$. Additionally, we see unexplained structures in $m(\Sigma_c^{++} \pi^- \pi^-)$ at $3.25 \text{ GeV}/c^2$, $3.8 \text{ GeV}/c^2$, and $4.2 \text{ GeV}/c^2$.

Combining our measurement with the results $\mathcal{B}(B^- \rightarrow \Sigma_c^0 \bar{p} \pi^+ \pi^-) = (4.4 \pm 2.0) \times 10^{-4}$ and $\mathcal{B}(B^- \rightarrow \Lambda_c^+ \bar{p} \pi^+ \pi^- \pi^-) = (22.5 \pm 6.8) \times 10^{-4}$ from CLEO [3], we calculate the resonant fractions $\frac{\mathcal{B}(B^- \rightarrow \Sigma_c^{++} \bar{p} \pi^- \pi^-)}{\mathcal{B}(B^- \rightarrow \Lambda_c^+ \bar{p} \pi^+ \pi^- \pi^-)} = (13.2 \pm 4.1) \%$ and $\frac{\mathcal{B}(B^- \rightarrow \Sigma_c^{++} \bar{p} \pi^- \pi^-) + \mathcal{B}(B^- \rightarrow \Sigma_c^0 \bar{p} \pi^+ \pi^-)}{\mathcal{B}(B^- \rightarrow \Lambda_c^+ \bar{p} \pi^+ \pi^- \pi^-)} = (33 \pm 13) \%$.

XI. Acknowledgments

We are grateful for the extraordinary contributions of our PEP-II colleagues in achieving the excellent luminosity and machine conditions that have made this work possible. The success of this project also relies critically on the expertise and dedication of the computing organizations that support *BABAR*. The collaborating institutions wish to thank SLAC for its support and the kind hospitality extended to them. This work is supported by the US Department of Energy and National Science Foundation, the Natural Sciences and Engineering Research Council (Canada), the Commissariat à l’Energie Atomique and Institut National de Physique Nucléaire et de Physique des Particules (France), the Bundesministerium für Bildung und Forschung and Deutsche Forschungsgemeinschaft (Germany), the Istituto Nazionale di Fisica Nucleare (Italy), the Foundation for Fundamental Research on Matter (The Netherlands), the Research Council of Norway, the Ministry of Education and Science of the

Russian Federation, Ministerio de Ciencia e Innovación (Spain), and the Science and Technology Facilities Council (United Kingdom). Individuals have received support from the Marie-Curie IEF program (European Union) and the A. P. Sloan Foundation (USA).

* Now at the University of Tabuk, Tabuk 71491, Saudi Arabia

† Also with Università di Perugia, Dipartimento di Fisica, Perugia, Italy

‡ Now at the University of Huddersfield, Huddersfield HD1 3DH, UK

§ Deceased

¶ Now at University of South Alabama, Mobile, Alabama 36688, USA

** Also with Università di Sassari, Sassari, Italy

- [1] K. Nakamura *et al.* (Particle Data Group), *J. Phys.* **G37**, 075021 (2010).
- [2] Throughout this paper, all decay modes represent that mode and its charge conjugate.
- [3] S. A. Dytman *et al.* (CLEO Collaboration), *Phys. Rev.* **D66**, 091101 (2002).
- [4] K. S. Park *et al.* (Belle Collaboration), *Phys. Rev.* **D 75**, 011101 (2007).
- [5] D. J. Lange, *Nucl. Instrum. Meth.* **A462**, 152 (2001).
- [6] S. Agostinelli *et al.* (GEANT4 Collaboration), *Nucl. Instrum. Methods* **A506**, 250 (2003).
- [7] B. Aubert *et al.* (*BABAR* Collaboration), *Nucl. Instrum. Methods* **A479**, 1 (2002).
- [8] B. Aubert *et al.* (*BABAR* Collaboration), *Phys. Rev.* **D 66**, 032003 (2002).
- [9] T. Allmendinger *et al.*, arXiv:1207.2849 [hep-ex] (submitted to *Nucl. Instrum. Methods*).